WETTING PROPERTIES OF STRUCTURED INTERFACES COMPOSED OF SURFACE-ATTACHED SPHERICAL NANOPARTICLES

A thesis submitted in a partial fulfillment
of the requirements for the degree of
Master of Science in Renewable and Clean Energy Engineering

by

BISHAL BHATTARAI
B.E., Visvesvaraya Tech University, India, 2015

2018
Wright State University

Wright State University
Graduate School

November 20, 2018

I HEREBY RECOMMEND THAT THE THESIS PREPARED UNDER MY SUPERVISION BY Bishal Bhattarai ENTITLED Wetting Properties of Structured Interfaces Composed of Surface-Attached Spherical Nanoparticles BE ACCEPTED IN PARTIAL FULFILLMENT OF THE REQUIREMENTS FOR THE DEGREE OF Master of Science in Renewable and Clean Energy Engineering.

_____
Nikolai V. Priezjev, Ph.D.
Thesis Director

_____
Joseph C. Slater, Ph.D., P.E.
Chair, Department of Mechanical and Materials Engineering

Committee on final examination

_____
Nikolai V. Priezjev, Ph.D.

_____
Ahsan Mian, Ph.D.

_____
Hong Huang, Ph.D.

_____
Sheng Li, Ph.D.

_____
Barry Milligan, Ph.D.
Interim Dean of the Graduate School

ABSTRACT

Bhattarai, Bishal. M.S.R.C.E., Department of Mechanical and Materials Engineering, Wright State University, 2018. *Wetting Properties of Structured Interfaces Composed of Surface-Attached Spherical Nanoparticles*.

In this thesis, the effects of the external pressure and surface energy on stability and wetting transition at nanotextured interfaces are studied using molecular dynamics and continuum simulations. The surface roughness of the composite interface is modeled via an array of spherical nanoparticles with controlled wettability. It was found that in the absence of external pressure, the liquid interface is flat and its location relative to the solid substrate is determined by the radius of the particle and the local contact angle. With increasing pressure on the liquid film, its interface becomes more curved and the three-phase contact line is displaced along the spherical surface but remains stable due to the re-entrant geometry. It was demonstrated that the results of molecular dynamics simulations for the critical pressure of the Cassie-Baxter wetting state agree well with the estimate of the critical pressure obtained by numerical minimization of the interfacial energy using Surface Evolver.

Contents

List of Figures

Acknowledgement

I am grateful to my supervisor Dr. Nikolai V. Priezjev for providing me this wonderful opportunity to work with him in his lab. I am thankful to his guidance, positive criticism and encouragement, especially when I had a very little idea about research.

Thanks to Mike Van Horn for his help in setting up computer and software and fixing other technical issues when needed.

Thanks to my friends who always supported me during my studies and with their encouraging ideas. Special thanks to my family who has taught me be cheerful even in hard times and for their motivation.

The analysis of liquid interfaces was performed in publicly available software, *Surface Evolver,* developed by Prof. K. A. Brakke at Susquehanna University. Prof. K. A. Brakke helped me understand the software also gave me the design ideas via email.

CHAPTER 1

Introduction

1.1 Literature Review

In the last few decades, the field of nanotechnology has attracted many scientists to study fundamental aspects of nanoscience and to apply this knowledge in many developing areas including medicine, materials design, water filtration, etc. Current progress in designing and making the so-called *superhydrophobic* surfaces has led to the production of composite surfaces with impressive and unusual properties, for example, self-cleaning surfaces, non-fouling surfaces, drag reduction, etc. [1]. This technology is useful from items in the household to big industrial products. For example, this can be applied to the kitchen dishes, so that water doesn't collect, preventing it from rusting, and for solar panels, to keep it clean, so that they can work with its maximum efficiency. In fact, we can also see this phenomenon in nature, for example, a lotus leaf uses it's superhydrophobic properties for self-cleaning and from risk of getting contagious disease [2]. Such surfaces can enable an improved control and operation of the liquid flow in nanofluidic and microfluidic systems [4-6]. In particular, it was demonstrated that laminar flows over variable textured surfaces can be in general described by the mobility tensor which relates the normal traction at the interface and the effective slip velocity [7]. A detailed comparison between continuum and atomistic simulations, showed that the effective slip boundary conditions and the velocity profiles agreed well when the dimensions of the surface patterns are greater than the liquid

molecular size [8, 9]. Superhydrophobic surfaces at the nano and microscales exhibit pillars-like textures. These pillars reduce the effective surface area that the liquid actually touches the substrate and retain the liquid film suspended at the tips of the pillars. Such structures generally have high contact angle (greater than 150 degrees) and low contact angle hysteresis (about 5 degrees). The two models, Wenzel and Cassie-Baxter have been largely used to describe the superhydrophobic properties. In the Wenzel model, the liquid fills the gap between the pillars and touches the substrate, whereas in the Cassie-Baxter model, the liquid only partially touches the pillars and the interface is separated from the lower substrate by the trapped air, thus forming a liquid-air-water interface. In general, the Wenzel state is characterized by lower apparent contact angle and higher contact angle hysteresis than the Cassis-Baxter state. The apparent contact angle at a composite interface is given by the Cassie-Baxter equation:

$$\cos\theta_c = (1 - f)\cos\theta - f, \quad (1)$$

where f is the liquid-air interface areal fraction and θ is the *intrinsic* contact angle of a liquid droplet at a smooth surface of the same material. Notably, Eq. (1) implies that the apparent contact angle becomes nearly 180 degrees, when the areal fraction f becomes closer to 1. However, there should be sufficiently small lateral separation between surface protrusions to allow the liquid-air interface to remain suspended locally above the surface; otherwise, the liquid wets the substrate fully. Thus, there are a number of factors, such as the breakthrough pressure that is required to fully wet the substrate, fragility of the surface texture, fluid temperature, and fouling resistance, that limit the applicability of superhydrophobic surfaces [3].

Similar to superhydrophobic cases, surfaces that display high contact angle (greater than 150 degrees) and low contact angle hysteresis (about 5 degrees) for the liquids with low surface tension, like oils and alcohols, are considered to be *superoleophobic*. Moreover, surfaces that display liquid contact angles greater than 150° along with low contact angle hysteresis (about 5 degrees) for liquids with both high and low surface tension values (for example, water and oil) are

termed as *superomniphobic* surfaces [10, 11]. The re-entrant curvature can be introduced to achieve such surfaces, when the three-phase contact line is stabilized at the concave regions of the solid curvature and the liquid interface remains suspended between surface protrusions above the solid substrate. Furthermore, in the Cassie-Baxter state, one can obtain better stability by imposing nanoscale texture on the microscale protrusions and a combination of many concave and convex segments might be involved [12]. Recently, the method of minimizing surface free energy and the potential energy of the external pressure was utilized for the equilibrium analysis and the stability of Cassie-Baxter wetting states at microstructured surfaces [13, 14]. The study of the critical external pressure, required to overcome the Laplace pressure due to the curved interface, was obtained for different 3D microstructures [13, 14]. However, the shape of the liquid interface with respect to the critical pressure when transforming from the Cassie-Baxter to Wenzel states on structured surfaces had not been be determined numerically.

In the past few years, the wetting properties of the liquid droplets on nanotextured surfaces were extensively studied using molecular dynamics simulations [15–25]. For example, it was shown that for larger height of pillars on the hydrophobic surface, the free-energy barrier for the Wenzel-to-Cassie state transition is much higher than from the Cassie-to-Wenzel state [15]. Also, there is a sensitive dependence of the apparent contact on the shape of the pillar cross-section and its height, pillars distance relative to each other, crystal plane orientation at the tops of the pillars, and the energy of interaction between pillar atoms and droplet molecules [15, 18, 20, 22 –24]. Interestingly, when the liquid droplet moves laterally over deformable pillar-arrayed substrate, the flexible hydrophilic pillars can accelerate the liquid upon approach and pin the receding contact line [19]. Moreover, it was recently revealed that one of the factors affecting wetting transition of a water droplet at a pillar-arrayed surface is the charge density at the base substrate [22]. However, the atomic details of the wetting transition with re-entrant surface curvature at nanostructured surfaces remain not fully understood, despite considerable computational efforts.

In this study, molecular dynamics and continuum simulations were utilized to investigate the effects of external pressure and surface energy on the wetting transition with re-entrant curvature at nanotextured surfaces. We considered polymeric liquid film partially wetting the surface of a spherical particle which is fixed rigidly at a solid substrate. It is shown the liquid/vapor interface position is determined by the radius of the particle and the local contact angle at surface of the particle. The interface remains flat when there is no external pressure. At zero pressure, the position of the liquid-vapor interface is determined by the local contact angle, i.e., the angle between the liquid interface and the solid sphere. With the application of the external pressure, the interface becomes curved and the degree of curvature is proportional to the external pressure. When the pressure reaches the critical value, the interface touches the substrate. We obtained an excellent agreement between the results of atomistic simulations and numerical minimization of the surface energy for the critical pressure with respect to the local contact angle.

1.1 Thesis Outline

The outline of the thesis is as follows:

Chapter 2 provides the description of molecular dynamics and continuum simulations.

Chapter 3 presents the correlation between the local contact angle and the surface energy of a liquid droplet on a flat substrate, and the dependence of pressure on the shape and location of the suspended liquid film. Also, the critical pressure as a function of the contact angle is analyzed.

Chapter 4 gives the summary of the results.

CHAPTER 2

Details of Numerical Simulations

2.1 Molecular Dynamics (MD) simulation model

Wetting properties of structured interfaces with an array of spherical particles on a solid substrate and a suspended liquid film is studied, as shown schematically in Fig.1. Molecular dynamics simulations were carried out on large scales using the parallel code LAMMPS developed at Sandia National Laboratories [26]. In this model, any two atoms interact through the truncated Lennard-Jones (LJ) potential represented by the equation:

$$V_{LJ}(r) = 4\varepsilon \left[\left(\frac{\sigma}{r}\right)^{12} - \left(\frac{\sigma}{r}\right)^{6} \right], \quad (2)$$

where ε and σ indicates the energy and length scales of the liquid phase, respectively. Also, the parameters ε_{wf} and σ_{wf} that are measured in units of ε and σ, respectively, describe the interaction between liquid molecules and solid atoms via the LJ potential. There are fixed solid atoms either on lattice sites or at the surface of a sphere and they do not interact with each other. Furthermore, we choose the same size for both liquid and solid atoms, i.e., $\sigma_{wf} = \sigma$. For computational efficiency, we set the cutoff radius to be $r_c = 2.5\sigma$ for interactions between fluid-fluid and fluid-solid molecules.

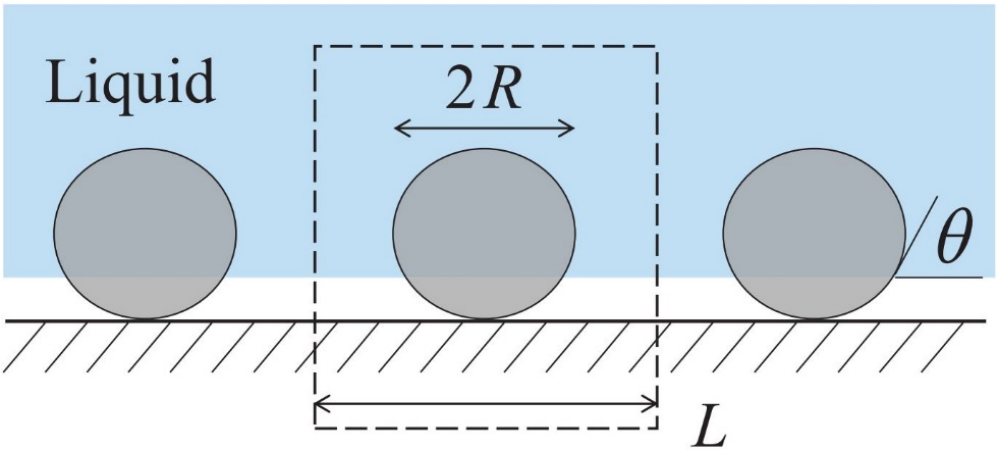

FIG. 1: (Color online) A schematic figure of the structured interface consisting of a collection of spherical protrusion attached with the solid substrate and a suspended thin liquid layer. θ indicates the local contact angle between the liquid interface and the surface of the solid particle. The dashed box used in molecular dynamics and continuum simulations represents the spatial domain.

Polymeric fluid, with atoms connected to form linear chains with N_p=10 atoms, was considered. In addition to the LJ potential, we used the FENE (finitely extensible nonlinear elastic) potential to describe the interaction between nearest neighbor atoms in a linear polymer chain

$$V_{FENE}(r) = -K/2\ r_o^2 \ln[1-r^2/r_o^2], \quad (3)$$

where the parameters are set to $k = 30\ \varepsilon\sigma^{-2}$ and $r_o = 1.5\ \sigma$ [28]. Thus, an effective harmonic potential is obtained from the combination of the LJ and FENE potentials parametrization that allows vibration of nearest neighbors but does not allow polymer chains to cross each other [28]. We also comment that in the present study, relatively short polymer chains considered to form a polymer melt well below the entanglement limit of about 70 beads per chain [28]. A constant temperature of 1.0 ε/k_B (k_B denotes the Boltzmann constant throughout) was used for the MD simulations, which was maintained via the Nose-Hoover thermostat applied to the fluid phase [26]. At this temperature, the dependence of the surface tension of a flat liquid/vapor interface as a function of the chain length was reported in Ref. [34]. The solution of the equations of motion were performed numerically using the velocity Verlet integration algorithm [26, 27] with the time step $\Delta t_{MD} = 0.005\ \tau$, where $\tau = \sigma\sqrt{m/\varepsilon}$ is the characteristic LJ time.

Our computational domain has the liquid film in contact with a solid sphere, which is rigidly fixed on a solid substrate as indicated by the dashed box in Fig. 1. Total 2500 atoms are arranged on square lattice sites within the *xy* plane and have dimensions $L \times L = 50.0\ \sigma \times 50.0\ \sigma$, on the solid substrate, and therefore, the areal density is 1.0 σ^{-2}. There is a fixed interaction energy of 1.0ε of the fluid monomers and atoms of the lower stationary substrate. Second, there are 4000 atoms uniformly distributed on a surface of a sphere with

the radius $R = 17.8\,\sigma$ on the solid particle, and, thus, with the areal density of $1.0\,\sigma^{-2}$. Thus, the LJ interaction energy between its atoms and fluid monomers, i.e., ε_{wf}, is the important input parameter controlling wetting properties of the solid sphere.

Next, we used 85000 monomers that altogether form 8500 polymer chains for the fluid. Parallel to the stationary lower substrate, periodic boundary conditions were imposed in the x and y directions. In MD simulations, the fluid phase is confined from above by the upper wall (not shown in Fig. 1), that consists of 2500 atoms arranged on a square plane with the linear size $L = 50.0\,\sigma$. The LJ interaction energy is also set to $1.0\,\varepsilon$ between fluid monomers and atoms of the upper wall. Unlike the stationary lower substrate, the upper wall is allowed move freely under the external pressure P, which is applied along the z (downward) direction toward the solid substrate, and under the forces from the fluid atoms. Thus, taking this geometry into consideration, the two parameters i.e., ε_{wf} and P, are used to determine the position of the liquid film relative to the stationary substrate and shape of the liquid-vapor interface. We finally comment that the effect of gravity was not considered in the present study.

2.2 Continuum simulations using Surface Evolver

The numerical simulation using the software, Surface Evolver was performed as a complimentary approach to analyze a liquid film trapped by the surface of a spherical particle [29]. C programming is used in the software and it uses a gradient decent method to gradually evolve the liquid surface towards minimum energy, subject to constraints. To

compare the results with the MD simulation, the same ratio of the sphere radius and the linear size of the simulation cell, *R/L,* was used in the problem shown in Fig. 1, as the one used in the MD setup. We define the unit cell of length L = 2.7322·R (where R is the radius of the spherical protrusion). Thus, the ratio, R/L = 0.366 is chosen to be similar in both the continuum and MD simulations. The geometry elements that represent surface in Surface Evolver are vertices, edges, facets and bodies, which are created in the text editor. The datafile body list begins with the keyword BODIES and it is followed by one body specification with the list of signed facet numbers. We put negative faces for the liquid surface since the liquid body is above the interface. Pressure is applied downwards in the negative z-direction and can be placed in the bodies section by adding a pressure attribute in the datafile. If a body is given a prescribed pressure, it contributes to energy, which is the given pressure times the actual volume of the body. As the mean curvature corresponds to the applied pressure, this energy generates the surface of prescribed mean curvature which is equivalent to prescribing the pressure difference. Pressure value can be interactively changed with the '*b'* command.

We performed grid size independency check, and to obtain stable results, we performed the calculations with sufficiently refined grid size, i.e., with 11760 facets. The grids are union of three edges or are triangular in shape. Periodic boundary conditions in the horizontal *x* and *y* directions are defined by a Torus model by using the keyword TORUS_PERIODS in the datafile. Thus, from results of MD simulations, the contact angle as a function of the surface energy was used as an input parameter in the continuum analysis. In our computational domain, initially, the liquid-vapor interface resides on a solid sphere at a certain height. The position and the shape of the interface is actively

monitored for each applied pressure step up to the critical value. At a particular step, a slight increase in the pressure causes a transition of the interface from Cassis-Baxter state to Wenzel state and thus the critical pressure is calculated.

CHAPTER 3

Results

3.1 Results of molecular dynamics simulations

Liquid and solid phase densities and the interaction energy between fluid monomers and wall atoms are the factors that determine the local contact angle and shape of the vapor-liquid interface near the contact line [30–33]. In order to determine the local contact angle as a function of the surface energy, we first performed a series of separate MD simulations and considered a polymeric droplet in contact with a solid substrate. More specifically, there were 8500 bead-spring polymer chains, each of length $N_p = 10$, to compose the droplet, which was placed in contact with a solid substrate that contains 25600 atoms rigidly fixed on a square lattice with lateral dimensions 160.0 σ × 160.0 σ. As described in the previous section, the areal density of atoms is kept same for both on the solid substrate and on the solid spherical particle. Additionally, we kept the thermostatting procedure, interaction potentials, and the relative size of solid and fluid atoms same as described in section 2.1.

3.1.1 Liquid droplet residing on a surface with different surface energies

Below, we present typical examples of liquid droplets partially wetting solid substrate for selected values of the wall-fluid interaction energy in Fig. 2. The system was equilibrated at the temperature of 1.0 ε/k_B for at least 3×10^6 MD steps, for each value of the wall-fluid interaction energy ε_{wf}. It can be clearly observed that the shape of the liquid-vapor interface becomes less curved and there is an increase in the liquid-solid contact area, with higher surface energy. We comment that with further increasing wall-fluid interaction energy, $\varepsilon_{wf} > 1.0\ \varepsilon$, the flat liquid film uniformly covers the solid substrate with thickness of about $3 - 4\ \sigma$ (not shown).

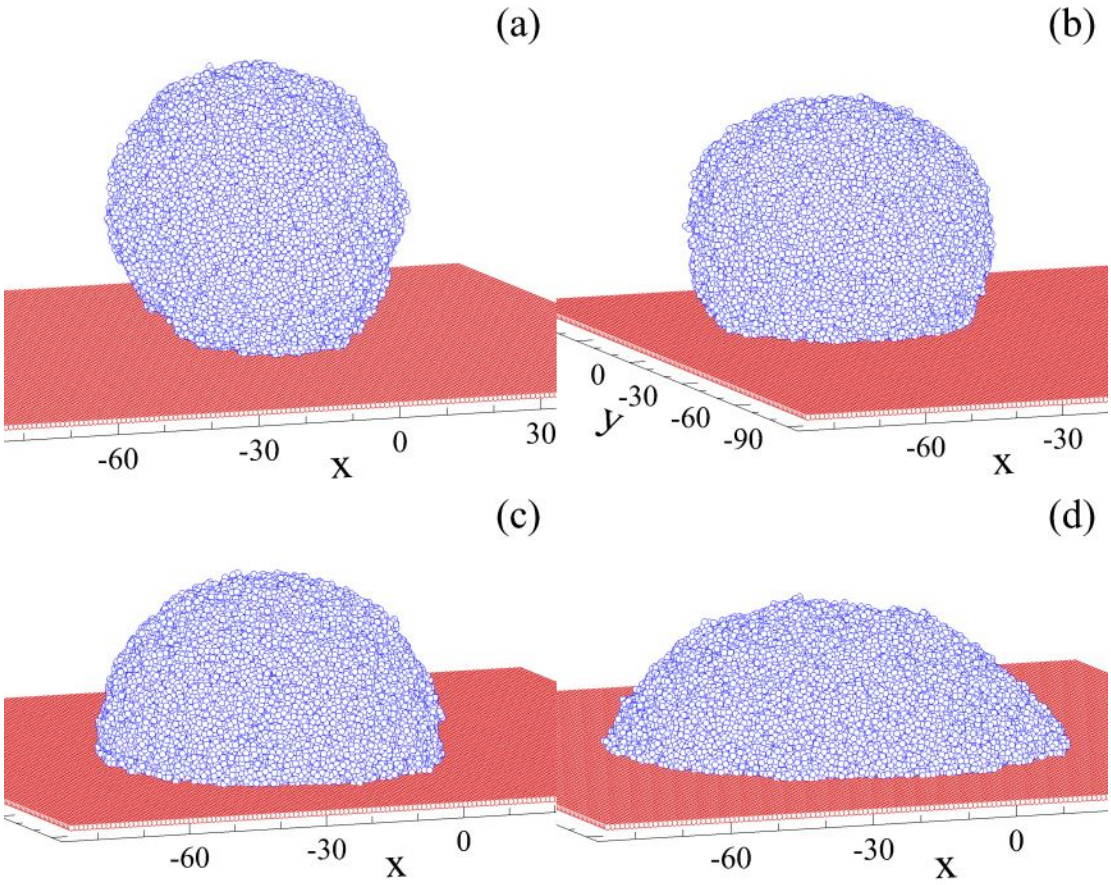

FIG. 2: (Color online) Snapshots of droplets consisting of 85000 atoms (blue circles), in contact with the solid substrate (red circles), with the interaction energy of wall and fluid (a) $\varepsilon_{wf} = 0.2\ \varepsilon$, (b) $\varepsilon_{wf} = 0.4\ \varepsilon$, (c) $\varepsilon_{wf} = 0.6\ \varepsilon$, and (d) $\varepsilon_{wf} = 0.8\ \varepsilon$. The solid substrate's dimensions are $160.0\ \sigma \times 160.0\ \sigma$.

3.1.2 Contact angle as a function of surface energy

To obtain the contact angle, we fitted a spherical cap to a liquid droplet and then for each value of ε_{wf}, an average over several independent configurations was taken. For different wall-fluid interaction energies, the summary of the data is shown in Fig. 3. We find, as expected, a monotonic decrease in the local contact angle, θ, from a large value of about 164.1°, in the case of droplet on a nearly nonwetting substrate to zero for a thin liquid film. The values of the local contact angle from the MD simulations were used as input parameters in the energy minimization method in the software Surface Evolver to model the shape of liquid interfaces around a solid spherical particle (described in section 3.2).

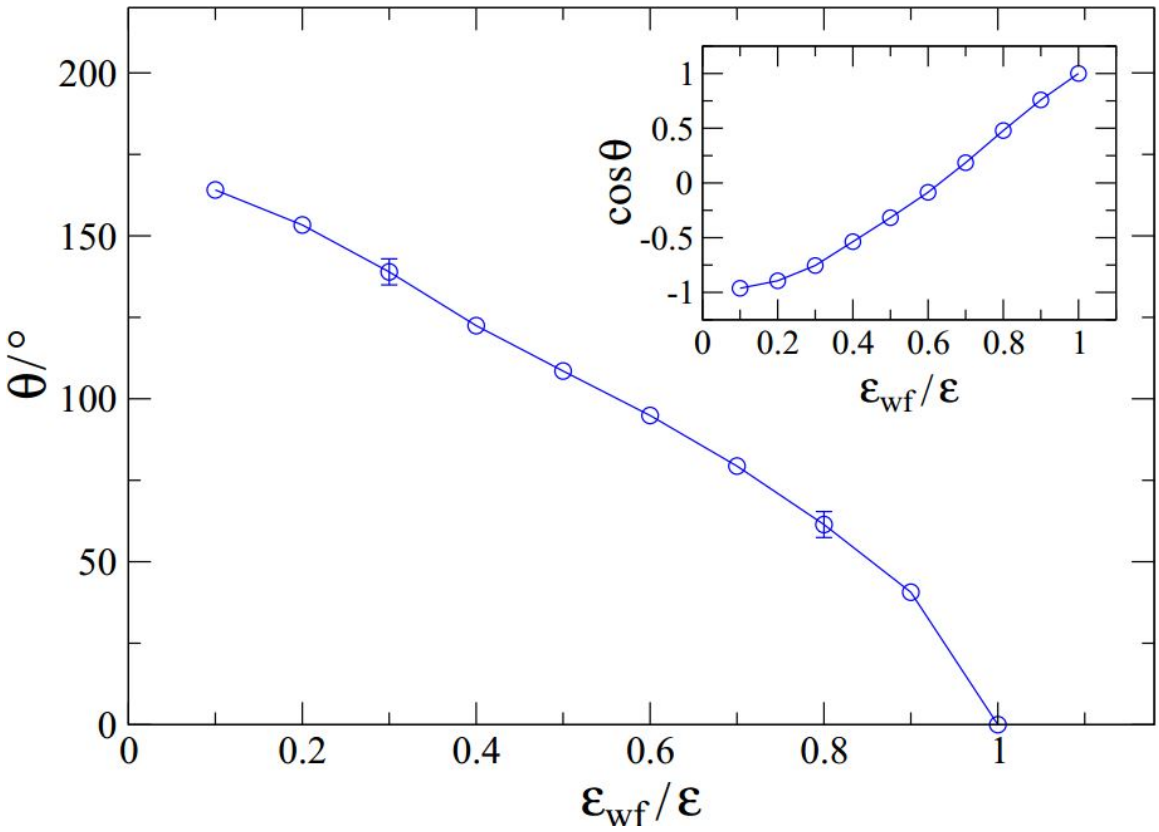

FIG. 3: (Color online) The relationship between the contact angle and the surface energy $\varepsilon_{wf}/\varepsilon$ for liquid droplets partially wetting a crystalline substrate. The data are obtained by fitting the liquid-vapor interface with a spherical cap. The inset shows the same data replotted as a function of cos $\theta(\varepsilon_{wf})$.

3.1.3 Liquid film suspended on a solid sphere

We next discuss the analysis of partially wetting states on textured surfaces covered by an array of solid spherical particles. We consider only one spherical particle, and the periodic boundary conditions were applied along the lateral directions to make the problem computationally feasible and to reduce the computation time, as shown in Fig. 1. The solid spherical particle is firmly attached to the lower solid substrate. The atoms of the solid substrate interact with the fluid monomers with the LJ energy of 1.0 ε. We extract two series of snapshots from the MD simulations as displayed in Fig. 4 for ε_{wf} =0.3 ε and in Fig. 5 for ε_{wf} =0.6 ε. On the upper wall (not shown), there was external pressure applied along the negative z direction. We performed calculations for the pressure increment of 0.05 ε σ^{-3} at each step. The time interval of 5 × $10^3\tau$ was chosen during which the liquid film and its interface were allowed to relax. Notice that there is the finite thickness of the liquid-vapor interface where some chain segments temporarily move away due to thermal fluctuations.

When there is no external pressure applied, the liquid-vapor interface is completely flat and its location with respect to the lower substrate is determined by the local contact angle, $\theta(\varepsilon_{wf})$, between the surface of the solid sphere and the interior of the liquid interface [see Fig. 4 (a) and Fig. 5 (a)]. As seen in Fig. 3, at lower surface energy, the local contact angle becomes larger, and, therefore, the liquid interface is located further away from the solid substrate in the case ε_{wf} =0.3 ε. It is clearly seen in Figs. 4 and 5 that the liquid-vapor interface becomes more curved and the liquid film is displaced closer to the solid substrate when the external pressure is increased. It can be seen that the liquid-vapor interface near

the corners of the simulation cell is more curved, located further away from the spherical particle and its periodic images.

For each value of the wall-fluid interaction energy, when the pressure is increased up to a critical value, we find that, first the sagged liquid/vapor interface touches the solid substrate, and finally triggers a transition to a fully wetting Wenzel state.

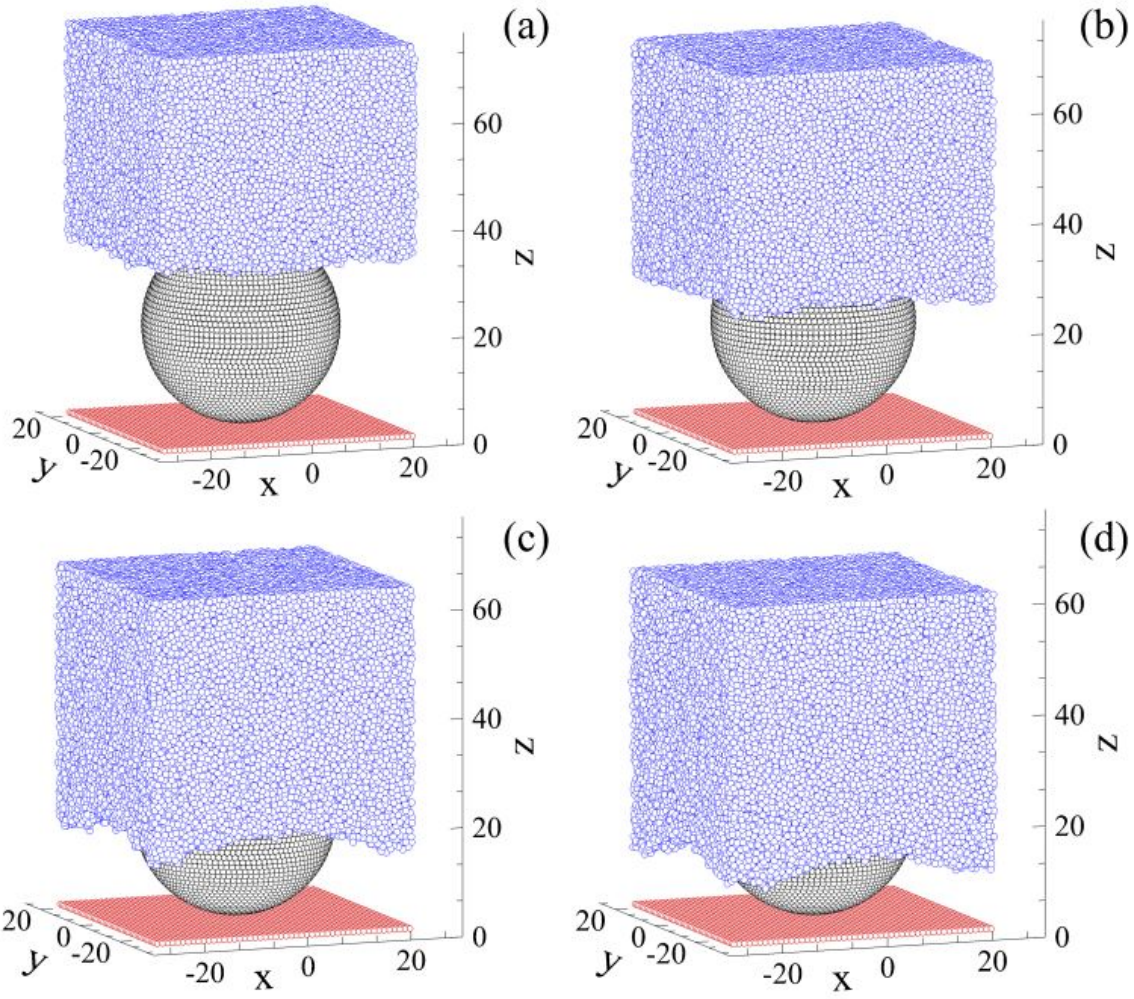

Fig. 4. Images from the snapshots of the suspended liquid film on the spherical particle. Here the wall-fluid interaction energy $\varepsilon_{wf} = 0.3\ \varepsilon$ and the vertical pressure (a) P =0, (b) P = $0.02\ \varepsilon\ \sigma^{-3}$, (c) P = $0.05\ \varepsilon\ \sigma^{-3}$, and (d) P = $0.055\ \varepsilon\ \sigma^{-3}$. The value of the averaged local contact angle is $\theta = 138.94°$.

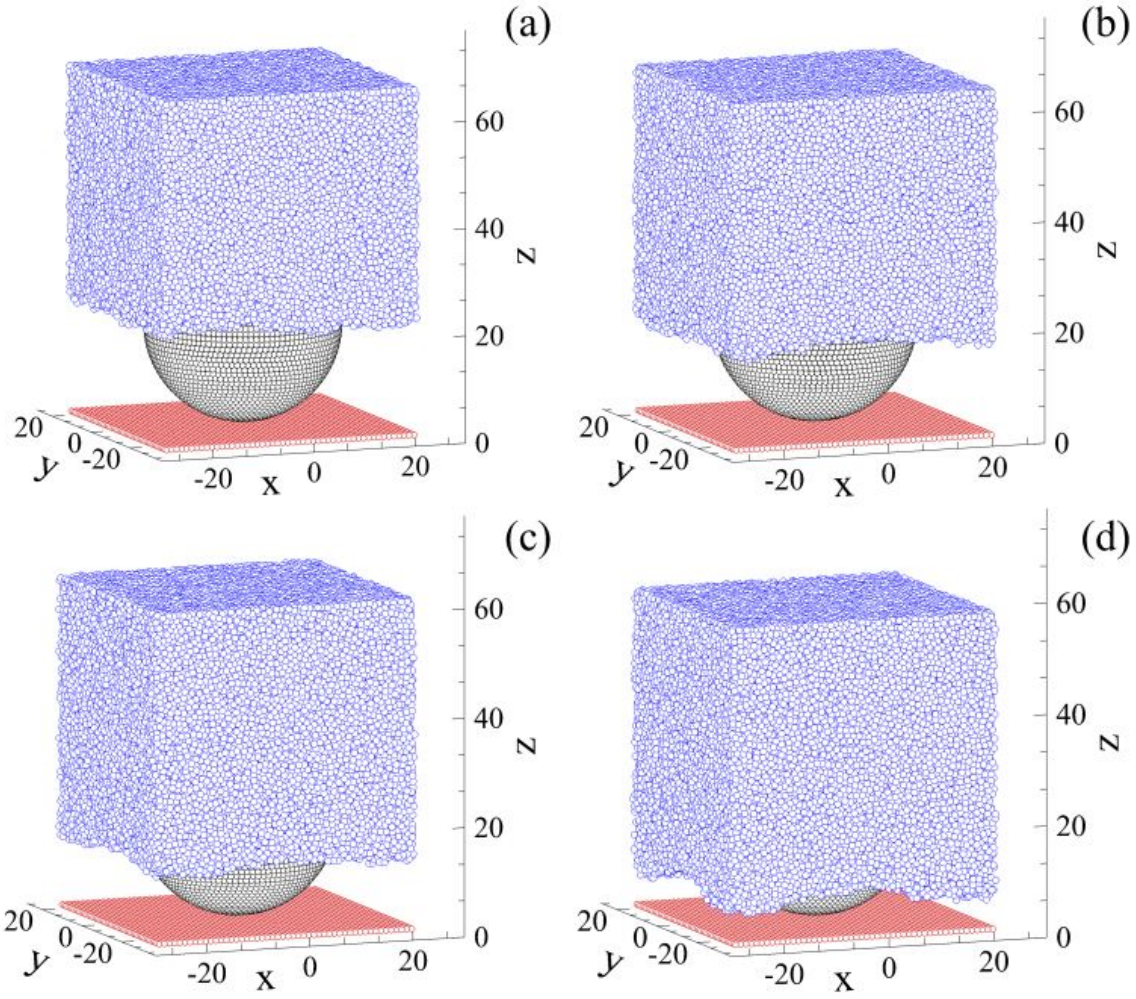

Fig. 5. Spherical particle wetted partially by the liquid film for the wall-fluid interaction energy $\varepsilon_{wf} = 0.6\ \varepsilon$ and the vertical pressure (a) P = 0, (b) P = 0.01 $\varepsilon\ \sigma^{-3}$, (c) P = 0.02 $\varepsilon\ \sigma^{-3}$, and (d) P = 0.03 $\varepsilon\ \sigma^{-3}$. Here, the average value of the local contact angle is $\theta = 94.86°$.

After completely wetting the spherical particle and the solid substrate, liquid film maintains the wetting state even if the external pressure is reduced. To put it simply, the wetting transition is permanent even upon reducing the external pressure down to zero. We present the variation of the critical pressure with the change in contact angle in Fig. 6. To remind the reader, the values of the local contact angle at the surface of the spherical particle were estimated from the spherical shape of the interface of a liquid droplet residing on a flat substrate, which has the same density as the solid particle (see Fig. 3). As evident from Fig. 6, the critical pressure increases for particles with more nonwetting properties. For more accuracy, the calculation was performed with the incrementation of the external pressure in smaller steps, by 0.01 $\varepsilon\ \sigma^{-3}$, in the vicinity of the wetting transition. Therefore, the maximum applied pressure at which the liquid interface remains suspended at the particle surface, for each value of θ, is also included in Fig. 6.

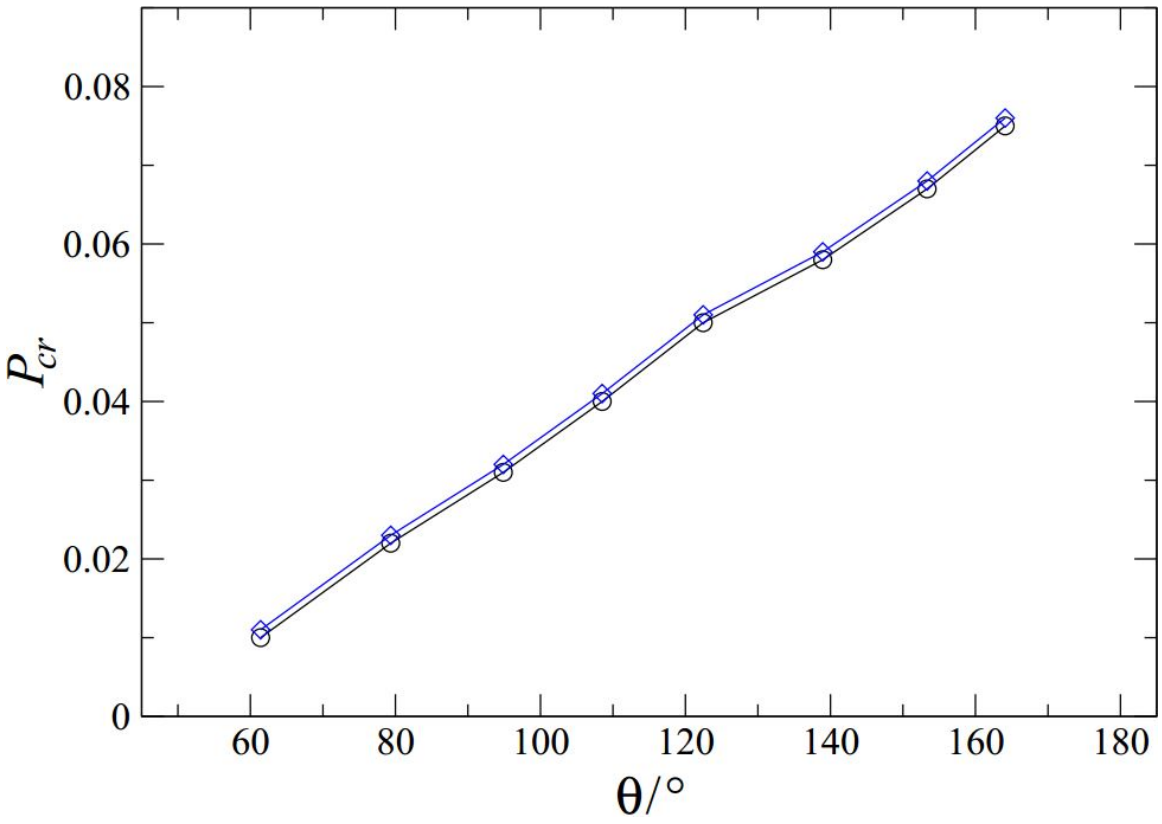

FIG. 6: (Color online) Relation between the critical pressure *Pcr* (units: $\varepsilon\ \sigma^{-3}$) with the local contact angle θ (degrees). Maximum external pressure (critical pressure) at which the liquid interface does not touch the solid substrate is represented by symbols (○). The threshold pressure for a wetting transition to the Wenzel state is indicated by symbols (◇).

3.2 Results of continuum simulations

We choose a complimentary approach to compare the results of molecular dynamics simulations of the critical pressure and the shape of three-dimensional liquid interfaces at structured surfaces. This method involves an energy minimization implemented in the software called Surface Evolver [29]. In this method, the surfaces of the lower solid substrate, solid spherical particle, and liquid interface are represented as a simplicial complex that consists of vertices, edges and facets. Grids are obtained by the union of edges that gives each grid a triangular formation.

3.2.1 Liquid droplet sitting on a solid substrate with different contact angles

Figure 7 shows the example of representative snapshots of liquid droplets that wet the solid substrate [35]. Similar to MD simulations, it can be observed that the solid-liquid contact area decreases with the increasing contact angle. This means that for larger surface energy, the solid-liquid contact area increases. Also, the surface of the droplet become more curved for higher values of the contact angle.

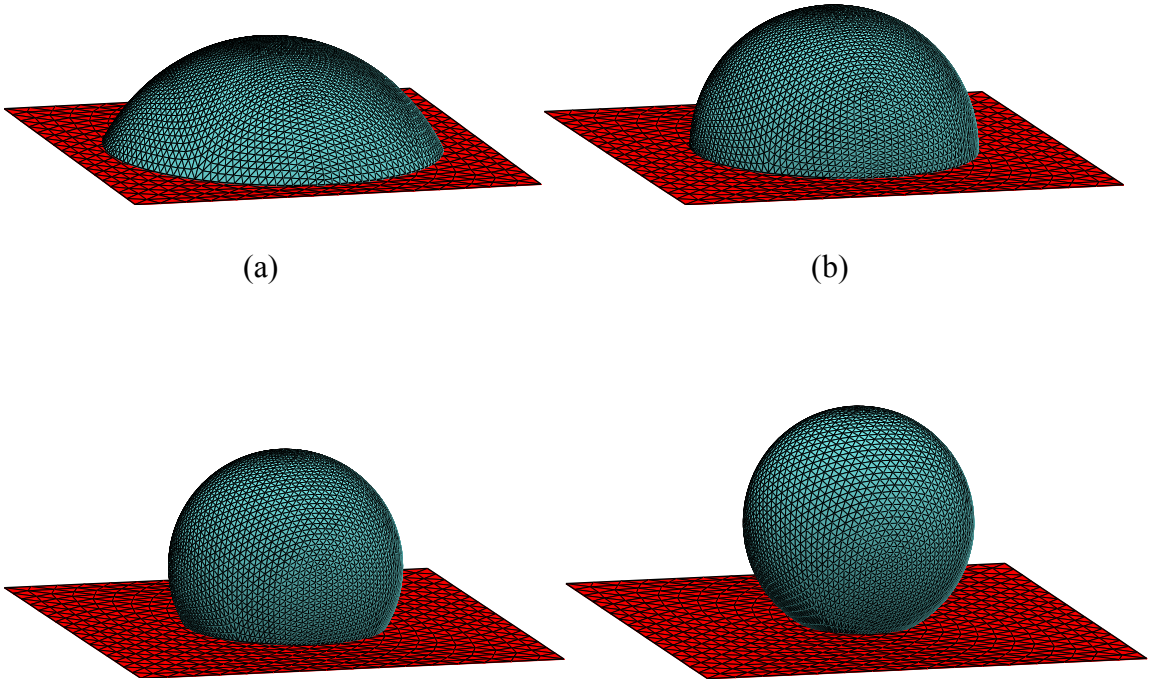

FIG. 7: Snapshots of liquid droplets (blue) in contact with the solid substrate (red) and solid-liquid contact angles (a) $\theta = 60°$, (b) $\theta = 90°$, (c) $\theta = 120°$, and (d) $\theta = 150°$.

3.2.2 Liquid interface suspended on a solid sphere

The liquid interface shown in Fig. 8 and Fig. 9 is a part of a suspended liquid film. In other words, the part of the liquid surface in the geometry under consideration is small enough and close enough to the center of the droplet that the actual size of the liquid droplet is not required for the computation. Similar to the MD setup, periodic boundary conditions were applied to the sideways in horizontal directions parallel to the solid substrate to represent a periodic array of spherical particles. Note that, in order to mimic the MD setup, we define the length of the unit cell $2.7322 \cdot R$ to obtain the ratio, $R/L = 0.366$ with 11760 facets. The spherical particle can be completely immersed into the liquid phase in the Wenzel state as this liquid volume is large enough. Using the gradient descent method, the liquid interface was evolved iteratively to the state with the lowest energy. We performed sufficiently large number of iterations so that the liquid interface is relaxed to form the local contact angle with the surface of the spherical particle as prescribed. The same values of the local contact angle as were reported in Fig. 3 were used in the continuum simulations.

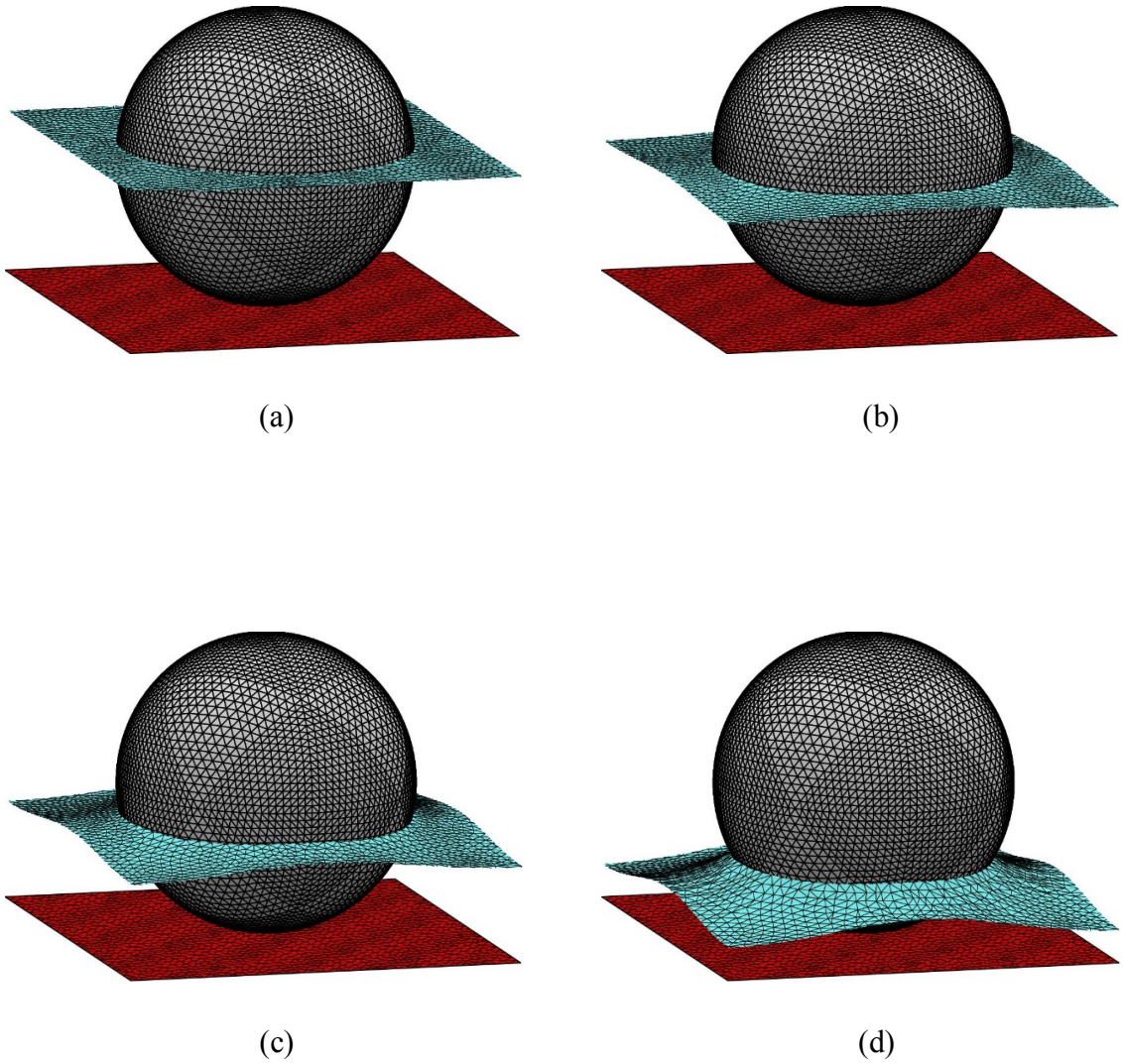

Fig. 8. Consecutive snapshots of the liquid-vapor interface obtained from the software Surface Evolver. The local contact angle between the surface of the solid sphere and the interior of the liquid interface is θ =94.86° and the surface tension coefficient is γ = 1.0 N/m. The external pressure applied are (a) P = 0, (b) P = 205 Pa, (c) P = 410 Pa, and (d) P = 610 Pa.

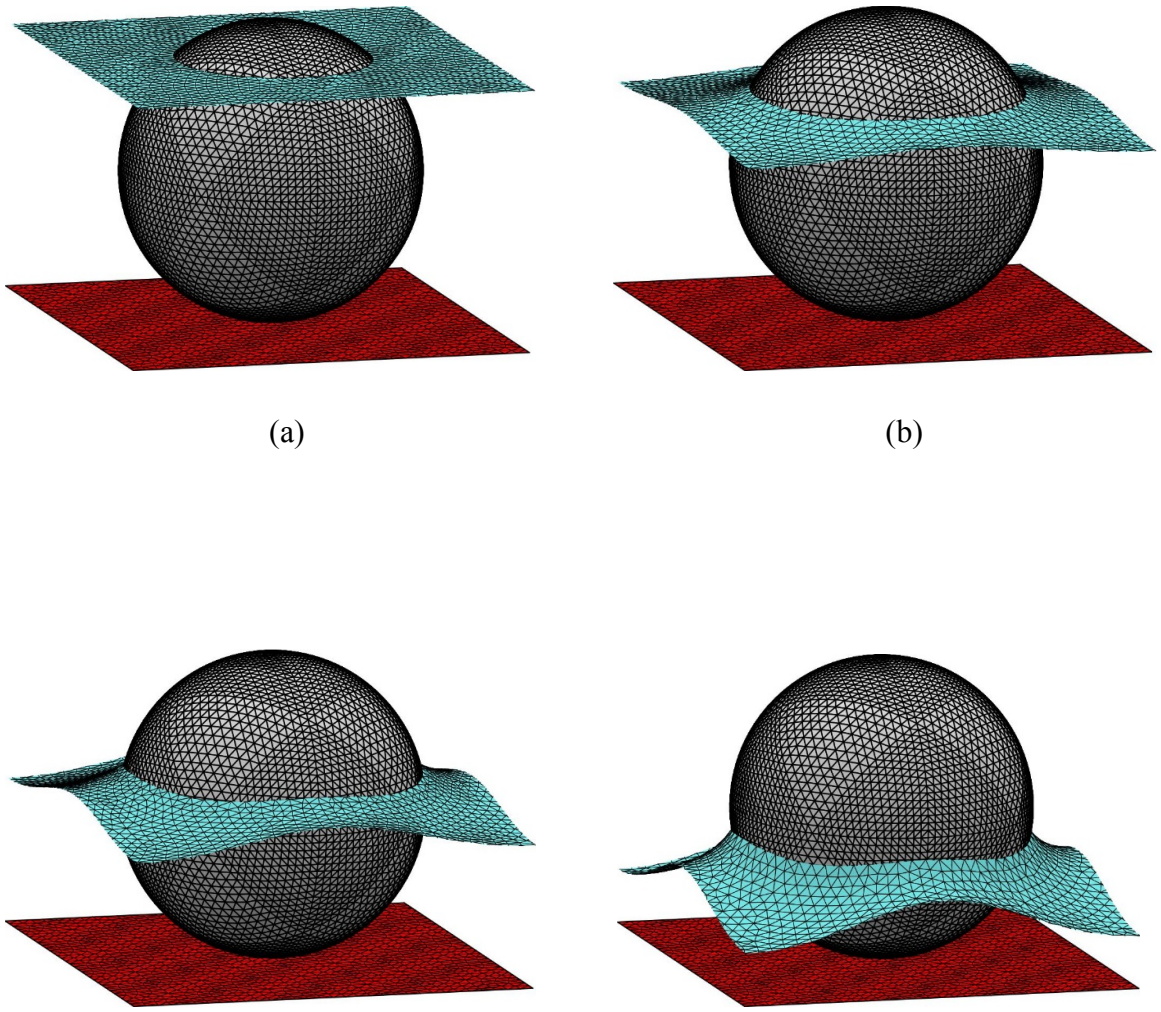

FIG. 9: (Color online) The shape of liquid-vapor interfaces with respect to the external pressures of (a) $P = 0$, (b) $P = 400$ Pa, (c) $P = 800$ Pa, and (d) $P = 1200$ Pa. The local contact angle at the surface of the spherical particle is $\theta = 138.94°$ and the surface tension of the liquid/vapor interface is $\gamma = 1.0$ N/m.

Typical snapshots of liquid/vapor interfaces around the solid spherical particle are shown, for two different local contact angles, in Fig. 8 for $\theta = 94.86°$ and in Fig. 9 for $\theta = 138.94°$ for the given values of the applied pressure. It can be observed that the liquid interface is flat when the external pressure is zero. When the pressure is applied, the interface starts to curve and at higher pressures, it becomes more curved and moves slightly towards the solid substrate. Upon further increasing external pressure, the liquid first touches the corner of the solid substrate of the simulation cell and then spreads at the solid substrate. Upon further iteration, this process continues until the interface forms a prescribed contact angle with the solid wall (not shown). For more accurate results, we increased the external pressure with a very small value near the critical pressure. The critical pressure of the wetting transition was determined with the accuracy of 0.5 Pa.

3.3 Comparison between the MD and continuum simulations

The results for the critical pressure obtained from MD simulations and energy minimization for different contact angles are summarized in Fig. 10. We used the dimensionless variable $P_{cr}L/\gamma$ to compare the simulation results, where L is the linear size of the solid substrate and γ is the surface tension coefficient. The input parameters were explicitly set to $L = 2.73$ mm and $\gamma = 1.0$ N/m in continuum simulation. By contrast, in MD simulations, the local contact angle is determined by the LJ interaction parameters and the surface tension need to be measured separately. The surface tension was estimated to be γ

= 0.85 ε/σ^2 for a thin liquid film that consists of bead-spring 10-mers at T = 1.0 ε/k_B and zero ambient pressure in the previous study [34].

The results for the critical pressure obtained from MD simulations and the continuum predictions agree well, as seen in Fig. 10. These results suggest that a continuum stability analysis might hold at length scales of about a few nanometers for partially wetting states at nanotextured surfaces. Thus, in our setup the nearest distance is about 30 molecular diameters between the surface of the spherical particle and its images. It should be also noted that one contributing factor to the slight discrepancy between two approaches is a finite cutoff radius of the LJ interaction potential between fluid molecules and solid atoms. In other words, a spontaneous wetting of the substrate due to thermal fluctuations might take place, if the sagged liquid/vapor interface is located within the cutoff radius from the solid substrate. We finally comment that in the present study, we considered only one value of the areal fraction, *i.e.*, $\phi_S = \pi R^2/L^2 = 0.42$. It is expected that the critical pressure is reduced due to smaller curvature of the liquid/vapor interface at the contact with the solid substrate with decreasing areal fraction [11].

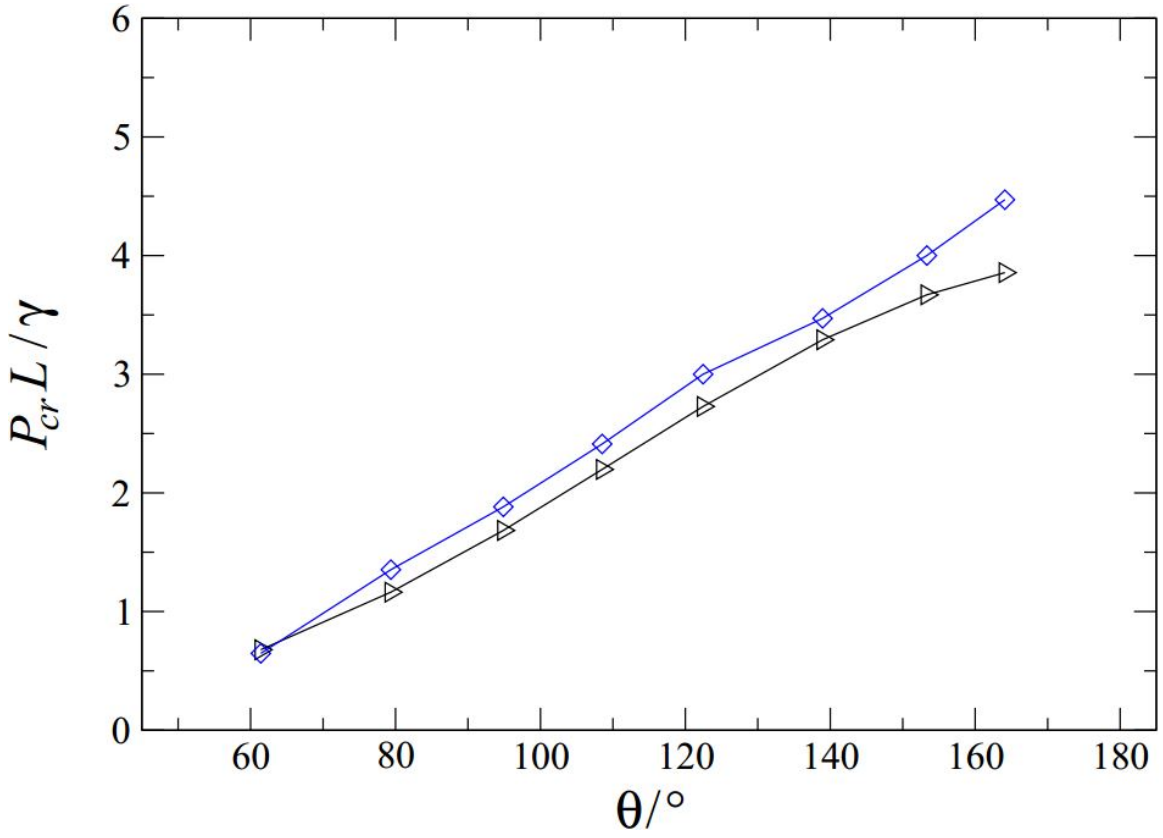

FIG. 10: The dimensionless variable $P_{cr}L/\gamma$ in relation with the local contact angle θ. The MD data and the results from continuum are indicated by (◇) and (⊳) respectively. Here, L is the length considered of the lower solid substrate and γ is the surface tension of the liquid-vapor interface. The error bars are about the size of the given symbol.

CHAPTER 4

Conclusions

In summary, we studied wetting properties of the composite interface consisting of a periodic array of spherical nanoparticles at the solid substrate, rigidly attached to it, by molecular dynamics simulations and numerical minimization of the interfacial energy using Surface Evolver. The strength of the energy of the fluid-solid interaction controls the wettability of spherical particles, which in turn determines the local contact angle. It was shown that when the applied pressure is zero, the liquid film remains suspended at the surface of solid particles and the distance of the film from the solid substrate is determined by the radius of the particle and the local contact angle. When there is an external pressure difference, the three-phase contact shifts accordingly. In other words, when the external pressure is gradually increased, the liquid film moves closer to the solid substrate but remains stable up to a critical value due to re-entrant curvature of the particle surface. It was found that there is an excellent agreement between the results of atomistic simulations and the numerical minimization of the interfacial energy for the shape of liquid interfaces and the critical pressure of permeation to the solid substrate. The results we found can be important for modeling partially wetting states on hierarchically textured surfaces that contain surface roughness on multiple length scales.

Bibliography

[1] A. K. Kota, C. Wonjae, and A. Tuteja, Superomniphobic surfaces: Design and durability. MRS Bulletin **38**, 383-390 (2013).

[2] H.-Y. Guo, B. Li, and X.-Q. Feng, Stability of Cassie-Baxter wetting states on microstructured surfaces. Physical Review E **94,** 042801 (2016).

[3] M. N. MacGregor-Ramiasa and K. Vasilev, Questions and answers on the wettability of nanoengineered surfaces, Adv. Mater. Interfaces **4**, 1700381 (2017).

[4] O. I. Vinogradova and A. L. Dubov, Superhydrophobic textures for microfluidics, Mendeleev Commun. **22**, 229 (2012).

[5] T. Lee, E. Charrault, and C. Neto, Interfacial slip on rough, patterned and soft surfaces: A review of experiments and simulations, Adv. Colloid Interface Sci. **21**, 210 (2014).

[6] C. Ybert, C. Barentin, C. Cottin-Bizonne, P. Joseph, and L. Bocquet, Achieving large slip with superhydrophobic surfaces: Scaling laws for generic geometries, Phys. Fluids **19**, 123601 (2007).

[7] M. Z. Bazant and O. I. Vinogradova, Tensorial hydrodynamic slip, J. Fluid Mech. **613**, 125 (2008).

[8] N. V. Priezjev, A. A. Darhuber, and S. M. Troian, Slip behavior in liquid films on surfaces of patterned wettability: Comparison between continuum and molecular dynamics simulations, Phys. Rev. E **71**, 041608 (2005).

[9] N. V. Priezjev, Molecular diffusion and slip boundary conditions at smooth surfaces with periodic and random nanoscale textures, J. Chem. Phys. **135**, 204704 (2011).

[10] A. Tuteja, W. Choi, M. Ma, J. M. Mabry, S. A. Mazzella, G. C. Rutledge, G. H. McKinley, and R. E. Cohen, Designing superoleophobic surfaces, Science **318**, 1618 (2007).

[11] A. Tuteja, W. Choi, J. M. Mabry, G. H. McKinley, and R. E. Cohen, Robust omniphobic surfaces, Proc. Natl. Acad. Sci. USA **105**, 18200 (2008).

[12] M. Nosonovsky and B. Bhushan, why re-entrant surface topography is needed for robust oleophobicity, Phil. Trans. R. Soc. A **374**, 20160185 (2016).

[13] B. Liu and F. F. Lange, Pressure induced transition between superhydrophobic states: Configuration diagrams and effect of surface feature size, J. Colloid Interface Sci. **298**, 899 (2006).

[14] H.-Y. Guo, B. Li, and X.-Q. Feng, Stability of Cassie-Baxter wetting states on microstructured surfaces, Phys. Rev. E **94**, 042801 (2016).

[15] T. Koishi, K. Yasuoka, S. Fujikawa, T. Ebisuzaki, and X. C. Zeng, Coexistence and transition between Cassie and Wenzel state on pillared hydrophobic surface, Proc. Natl. Acad. Sci. USA **106**, 8435 (2009).

[16] X. Yong and L. T. Zhang, Nanoscale wetting on groove-patterned surfaces, Langmuir **25**, 5045 (2009).

[17] T.-H. Yen, Investigation of the effects of perpendicular electric field and surface morphology on nanoscale droplet using molecular dynamics simulation, Molecular Simulation **38**, 509 (2012).

[18] J. K. Saha, M. A. Matin, J. Jang, and J. Jang, Molecular dynamics simulation study on the wetting behavior of a graphite surface textured with nanopillars, Bull. Korean Chem. Soc. **34**, 1047 (2013).

[19] Q. Yuan and Y.-P. Zhao, Wetting on flexible hydrophilic pillar-arrays, Sci. Rep. **3**, 1944, (2013).

[20] X. M. Xu, G. Vereecke, C. Chen, G. Pourtois, S. Armini, N. Verellen, W.-K. Tsai, D.-W. Kim, E. Lee, C.-Y. Lin, P. V. Dorpe, H. Struyf, F. Holsteyns, V. Moshchalkov, J. Indekeu, and S. De Gendt, Capturing wetting states in nanopatterned silicon, ACS Nano **8**, 885 (2014).

[21] Q. Yuan and Y.-P. Zhao, Statics and dynamics of electrowetting on pillar-arrayed surfaces at the nanoscale, Nanoscale **7**, 2561 (2015).

[22] A. M. Miqdad, S. Datta, A. K. Das, and P. K. Das, Effect of electrostatic incitation on the wetting mode of a nano-drop over a pillar-arrayed surface, RSC Adv. **6**, 110127 (2016).

[23] W. Xu, Z. Lan, B. L. Peng, R. F. Wen, and X. H. Ma, Effect of nano structures on the nucleus wetting modes during water vapour condensation: from individual groove to nanoarray surface, RSC Adv. **6**, 7923 (2016).

[24] C.-C. Chang, Y.-J. Sheng, and H.-K. Tsao, Wetting hysteresis of nanodrops on nanorough surfaces, Phys. Rev. E **94**, 042807 (2016).

[25] J. Yan, K. Yang, X. Zhang, and J. Zhao, Analysis of impact phenomenon on superhydrophobic surfaces based on molecular dynamics simulation, Comput. Mater. Sci. **134**, 8 (2017).

[26] S. J. Plimpton, Fast parallel algorithms for short–range molecular dynamics, J. Comp. Phys. **117**, 1 (1995).

[27] M. P. Allen and D. J. Tildesley, *Computer Simulation of Liquids* (Clarendon, Oxford, 1987).

[28] K. Kremer and G. S. Grest, Dynamics of entangled linear polymer melts: A molecular dynamics simulation, J. Chem. Phys. **92**, 5057 (1990).

[29] K. A. Brakke, The Surface Evolver, Experimental Mathematics **1**, 141 (1992).

[30] P. van Remoortere, J. E. Mertz, L. E. Scriven, and H. T. Davis, Wetting behavior of a Lennard-Jones system, J. Chem. Phys. **110**, 2621 (1999).

[31] A. Milchev, A. Milchev, and K. Binder, Nanodroplets on a solid plane: wetting and spreading in a Monte Carlo simulation, Comput. Phys. Comm. **146**, 38 (2002).

[32] E. Bertrand, T. D. Blake, and J. De Coninck, Influence of solidliquid interactions on dynamic wetting: a molecular dynamics study, J. Phys.: Condens. Matter **21**, 464124 (2009).

[33] J. H. Weijs, A. Marchand, B. Andreotti, D. Lohse, and J. H. Snoeijer, Origin of line tension for a Lennard-Jones nanodroplet, Phys. Fluids **23**, 022001 (2011).

[34] D. R. Heine, G. S. Grest, and E. B. Webb, Spreading dynamics of polymer nanodroplets, Phys. Rev. E **68**, 061603 (2003).

[35] K A. Brakke, Surface Evolver Manual, Version 2.70 (2013)